# Bound state of distant photons in waveguide quantum electrodynamics

Alexander V. Poshakinskiy[1] and Alexander N. Poddubny[2,*]
[1]*Ioffe Institute, St. Petersburg 194021, Russia*
[2]*Department of Physics of Complex Systems, Weizmann Institute of Science, Rehovot 7610001, Israel*

(Received 7 April 2023; accepted 25 July 2023; published 8 August 2023)

We study theoretically quantum eigenstates in an array of two-level atoms coupled to the waveguide. We show that this system features double-excited states where the two excitations are localized at the opposite edges of the array. Such bound states of distant excitations result from the long-ranged photon-mediated coupling in the waveguide setup, which mediates repulsion at larger distances. These results could be useful for the rapidly developing field of waveguide quantum electrodynamics, studying waveguide-coupled arrays of cold atoms or superconducting qubits.

DOI: 10.1103/PhysRevA.108.023707

## I. INTRODUCTION

The quantum-mechanical problem of a particle moving in one spatial dimension and confined in a box is probably the most paradigmatic model of quantum mechanics. A wave function of a single particle of mass $m$ in a box of size $N$ forms standing waves, $\psi(x) \propto \sin Kx$, where $K = \pi/N, 2\pi/N, \ldots$ and the energy levels are given by $\hbar^2k^2/2m$. The situation becomes more interesting in the many-body case, when several quantum particles are put in the box and are allowed to interact with each other. For example, the problem of bosons with strong repulsive interaction can be solved exactly and the composite many-body wave function is proportional to a Slater determinant of wave functions of noninteracting particles, e.g.,

$$\Psi(x_1, x_2) \propto \mathrm{sgn}(x_1 - x_2)[\psi_1(x_1)\psi_2(x_2) - \psi_2(x_1)\psi_1(x_2)]$$

for a pair of particles. The strong repulsion of bosons thus effectively emulates the Pauli exclusion principle, leading to a so-called fermionization [1]. Another possibility is offered by bound many-particle states. The two attracting particles can form a bound pair so that their joint probability will decay with the characteristic length $a$. Such bound pair can propagate as a whole with the center-of-mass wave vector $K$ and can be quantized in a finite box,

$$\Psi(x_1, x_1) \propto \sin\left(K\,\frac{x_1 + x_2}{2}\right)e^{-|x_1 - x_2|/a}.$$

One of the instructive examples of such states is presented by a bound electron-hole pair in a semiconductor, an exciton, that is confined in a quantum well [2]. If the well is wider than the exciton Bohr radius, the exciton is quantized as a whole. On the other hand, if the well width is smaller than the Bohr radius, the exciton is destroyed and electrons and holes are quantized independently, $\Psi(x_1, x_2) \propto \sin K_1x_1 \sin K_2x_2$, where $K_{1,2}$ are the wave vectors of the corresponding particles.

In this work, we consider yet another quantum state of two interacting particles in a box, that we term as "distant bound state," where the wave function has the form

$$\Psi(x_1, x_2) \propto e^{-x_1/a}e^{-|N - x_2|/a} + (x_1 \leftrightarrow x_2). \tag{1}$$

Such a state can be viewed as an entangled Bell state of particles, pinned by the interaction to the opposite sides of the box. Its origin of formation is qualitatively illustrated in Fig. 1. Suppose that in the semi-infinite arrays there exist single-particle edge states, $|L\rangle$ and $|R\rangle$, localized at the left and right edges, respectively. Due to the mirror symmetry, the eigenstates of the finite array will be the even and odd combinations $|\psi_\pm\rangle = (|L\rangle \pm |R\rangle)/\sqrt{2}$. Now we proceed to the double-excited states. Figures 1(a) and 1(b) illustrate the product states with both particles either in the state $|\psi_+\rangle$ or $|\psi_-\rangle$, namely $|\Psi_\pm\rangle = |\psi_\pm^{(1)}\rangle|\psi_\pm^{(2)}\rangle$. In the case of large structure, and when the interaction between the two particles is neglected, the states $|\Psi_\pm\rangle$ are degenerate. However, strong interaction between the particles can mix these product states leading to the formation of new even and odd combinations $|\chi_\pm\rangle = (|\Psi_+\rangle \pm |\Psi_-\rangle)/\sqrt{2}$, shown in Figs. 1(b) and 1(d). The even combination can also be interpreted as an edge state of the bound photon pair,

$$|\chi_+\rangle = \frac{1}{\sqrt{2}}(|L_1\rangle|L_2\rangle + |R_1\rangle|R_2\rangle), \tag{2}$$

where both particles are simultaneously localized either at the left or at the right edge of the structure (here, the subscripts 1, 2 denote the particle numbers). In this work, we focus on the odd combination

$$|\chi_-\rangle = \frac{1}{\sqrt{2}}(|L_1\rangle|R_2\rangle + |R_1\rangle|L_2\rangle), \tag{3}$$

which is an entangled Bell state of photons at the left and right edges of the array [Fig. 1(d)] and is equivalent to the distant bound state Eq. (1).

The key ingredient necessary to the formation of a state Eq. (1) is the strong interaction between the particles at a large distance, which is necessary to repel them from each

*poddubny@weizmann.ac.il

 

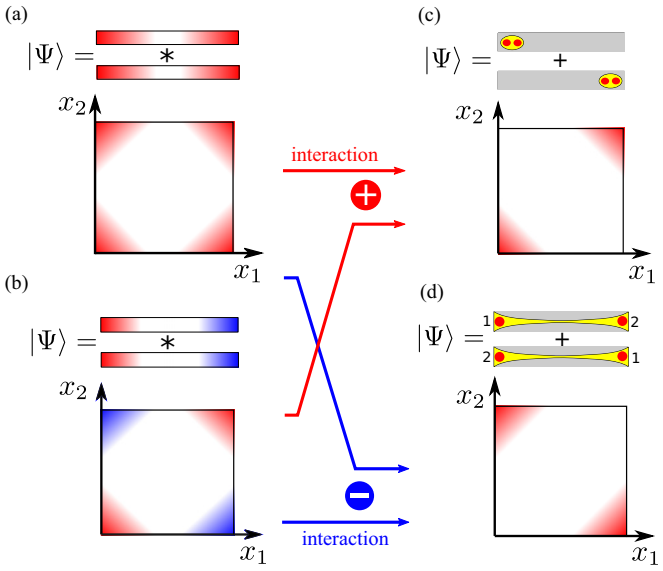


FIG. 1. Schematic illustration of two-photon wave functions for superpositions of even (a) and odd (b) single-particle edge states and their interaction-induced combinations: edge state of bound pair (c) and distant bound state (d). The false-color map shows the two-particle wave-function amplitude $\Psi(x_1, x_2)$ depending on their coordinates $x_1$ and $x_2$.

other. This requirement may seem challenging because the two particles, exponentially localized at the opposite edges of the structure, should hardly interact. Any significant repulsion, pushing them to the opposite edges, does not seem feasible. This should hinder formation of the distant bound states in the model with only nearest-neighbor coupling and short-range interactions. For example, the Bose-Hubbard models with nearest-neighbor coupling and short-range repulsion between the particles feature the edge bound states [3,4], similar to Fig. 1(c), but not the distant bound state. Edge-localized modes are also well known for the $XXZ$ spin chains with open boundary conditions [5,6], but we are not aware of the states of type Fig. 1(d). Very recently, such a state has been theoretically predicted for two interacting polaritons in a one-dimensional waveguide in the presence of the long-ranged dipole interaction between the two polaritons [7]. Here, we will show that the distant bound states can arise even in the presence of only short-range interactions.

We consider the setup of waveguide quantum electrodynamics (WQED), where an array of natural or artificial two-level atoms (such as superconducting qubits or quantum defects) is coupled to the waveguide [8–12]. The interactions between the excitations in this setup are induced by the anharmonicity of the two-level atom potential and are short ranged. On the other hand, the WQED setup has built-in long-ranged coupling between the atoms, mediated by the photons propagating in the waveguide. Our goal is to demonstrate that distant bound states Eq. (1) naturally arise in such a system and that they are robust against fluctuating short-range interactions between the atoms.

## II. NUMERICAL MODELING

We consider an array of equidistant two-level atoms coupled to a waveguide, schematically illustrated in the top inset in Fig. 2(b). The system is described by the following effective Hamiltonian, written in the Markovian approximation [13]:

$$H = -i\gamma_{1D} \sum_{n,m} \sigma_n^\dagger \sigma_m e^{i\varphi|m-n|}, \tag{4}$$

where the energy is counted from the atomic resonance $\omega_0$ (we assume $\hbar = 1$), $\sigma_n^\dagger$ are the atomic raising operators, and $\varphi = \omega_0 d/c$ is the phase gained by light traveling the distance $d$ between two neighboring atoms. The parameter $\gamma_{1D} \equiv \Gamma_{1D}/2$ is the radiative decay rate of a single atom into the waveguide. The key feature of the Hamiltonian Eq. (4) is the long-ranged waveguide-mediated coupling between the distant atoms. On the other hand, the interaction, that is quantum nonlinearity, is local and results from the fact that a given atom cannot be doubly excited, $\sigma_m^2 = 0$. We diagonalize the Hamiltonian Eq. (4) numerically in the domain of double-excited states $\sum_{n,m=1}^{N} \Psi_{nm} \sigma_n^\dagger \sigma_m^\dagger |0\rangle$ for finite $N$-atom arrays by solving the Schrödinger equation $H|\Psi\rangle = 2\varepsilon|\Psi\rangle$; see Ref. [10] for the derivation details. Figure 2 presents our results obtained numerically for a finite array with $N = 200$ atoms. The complex two-excitation energy spectrum is shown in Fig. 2(a). The imaginary part of the eigenenergy $\varepsilon$ describes the radiative losses into the waveguide. The points are colored according to the average photon-photon distance

$$\rho = \sum_{n,m=1}^{N} |n-m||\Psi_{nm}|^2 \tag{5}$$

and we also show the histogram of the photon-photon distances' distribution in Fig. 2(c). This distribution has a broad peak at $\rho \approx 70 \approx N/3$, corresponding to a pair of quasi-independent delocalized excitations. The tails of the distribution correspond to the bound photon pairs (small $\rho$) and distant bound states we focus on (large $\rho$). In order to provide more insight into the two-photon spectrum, we plot in Fig. 2(b) the wave functions of four characteristic two-photon states of different types. For example, the state No. 1 is close to a direct product of two symmetric combinations of left- and right-edge states, as shown in Fig. 1(a). The state No. 3 corresponds to both photons localized either close to the left or to the right edge of the array at the same time and can be qualitatively understood as an edge state of bound photon pair [Fig. 1(b)]. Our key observation in Fig. 2(a) is the existence of a large number of states, where the photon-photon distance $\rho$ is comparable with the system size (yellow-colored points). The two-photon wave function for the most distant state No. 2, with the largest value of $\rho$, is shown in Fig. 2(b). This state looks very similar to the Bell state of left- and right-edge photons, schematically illustrated in Fig. 1(d). Another kind of distant bound state with a slightly different wave function is the state No. 4.

We now analyze the two-photon spectrum in more detail. Our goal is to understand the origin of single-particle edge states, then to examine how their interaction leads to the formation of two-particle bound states, and finally demonstrate the robustness of the distant bound state against the disorder.

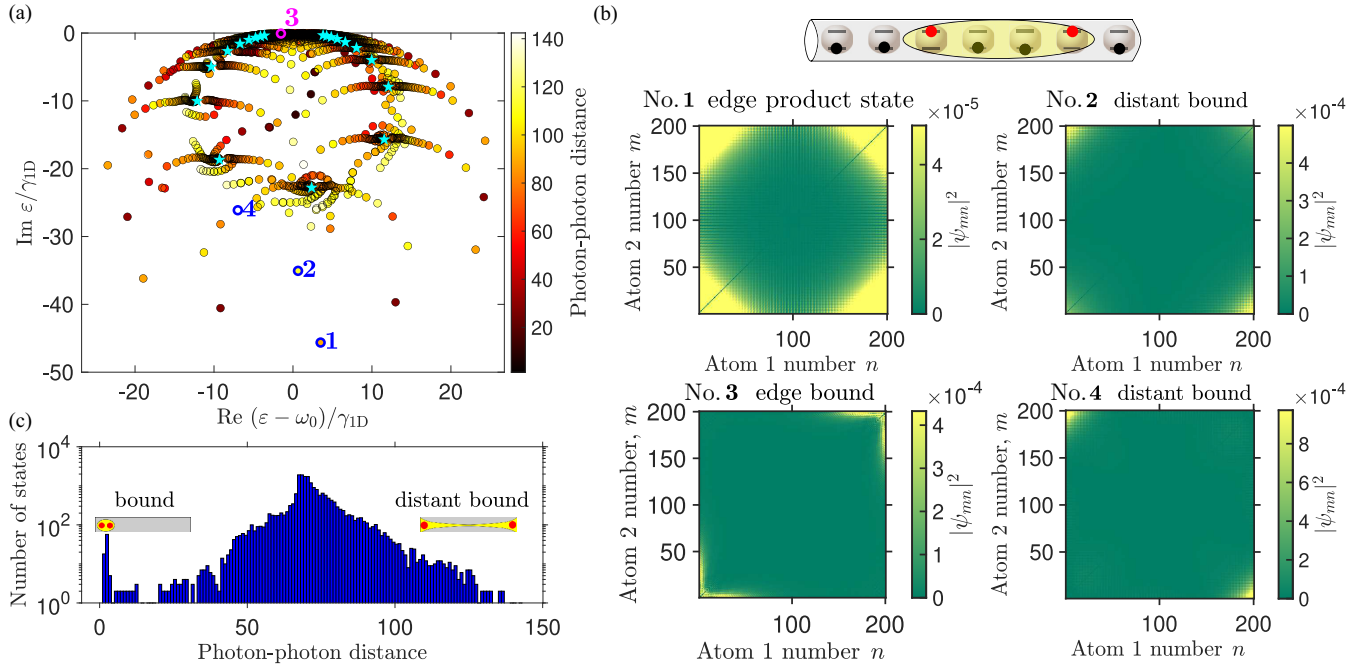


FIG. 2. Complex two-polariton energy spectrum of the array of $N = 200$ atoms. The color indicates the mean photon-photon distance $\rho$ calculated according to Eq. (5). Cyan stars show a single-polariton energy spectrum. (b). Color maps show probability distribution $|\psi_{nm}|^2$ for four characteristic two-polariton states with the energies $(\varepsilon-\omega_0)/\gamma_{1D} \approx 3.5$–$45.6i$, $-7.0$–$26.1i$, $11.1$–$19.9i$, $-1.6$–$0.1i$, respectively, indicated with the corresponding numbers in (a). Top inset shows schematics of the array of atoms coupled to the waveguide with two interacting excitations. (c) Histogram showing the distribution of the photon-photon distances $\rho$. Calculation has been performed for $N = 200$ and $\varphi \equiv \omega_0 d/c = 1$.

We start with the singular value decomposition of the distant bound state No. 2 from Fig. 2(b),

$$\Psi_{mn} = \sum_{\nu=1}^{N} \lambda_\nu \psi_n^\nu \psi_m^\nu, \tag{6}$$

where due to the bosonic symmetry $\Psi_{nm} = \Psi_{mn}$ left and right singular vectors coincide and can be chosen to satisfy the unconjugated orthogonality condition $\sum_{n=1}^{m} \psi_n^\nu \psi_n^\mu = \delta_{\mu\nu}$. The distribution of the 20 largest eigenvalues $\lambda_\nu$ is presented in Fig. 3(a). Due to the mirror symmetry, the singular vectors $\psi_n^\mu$ are either odd or even and we denote the corresponding singular values by blue and red color, respectively. Figure 3(b) shows the approximation to the wave function, calculated leaving only the four largest singular values corresponding to two odd and two even singular vectors in the expansion Eq. (6). Such two-term expansion well approximates the exact wave function No. 2 from Fig. 2(b). The localization of the distant bound state at the edges of the array can be explained by the fact that the single-particle eigenstates are also localized; compare two corresponding wave functions, shown in Fig. 3(c). These findings fully confirm our interpretation of the formation mechanism of the distant bound state illustrated in Fig. 1: it is formed due to the interaction-induced interference of the even and odd single-particle states localized at the opposite edges of the array.

It is also instructive to analyze the single-particle energy spectrum, obtained by solving the Schrödinger equation $H|\psi\rangle = \varepsilon|\psi\rangle$ with the ansatz $|\psi\rangle = \sum_{n=1}^{N} \psi_n \sigma^\dagger|0\rangle$ and shown in Fig. 2(a) by cyan stars. Eigenmodes of the finite array can be presented as a superposition of two polaritonic Bloch waves [14]:

$$\psi_n \propto r\, e^{iKn} + e^{-iKn}, \tag{7}$$

where $K$ is the polariton wave vector determined from the dispersion equation $\cos K = \cos\varphi - \gamma_{1D} \sin\varphi/\varepsilon$ and $r = -(1 - e^{i(\varphi-K)})/(1 - e^{i(\varphi+K)})$ is the internal reflection coefficient of polaritons from the edge of the array. Due to the radiative losses, the polariton eigenfrequencies $\varepsilon$ in the finite array and the corresponding wave vector $K$ are complex. The states with the largest radiative decay rate have the real part of the wave vector $\mathrm{Re}\, K(\varepsilon)$ close to $\pm\varphi$, which can be understood as a kind of phase synchronism condition facilitating photon emission [15]. The phase synchronism is also evident from the Fourier transform of the two-photon wave function $\psi_{k_x,k_y} = \sum_{m,n=1}^{N} e^{-ik_x m - ik_y n} \Psi_{mn}$, shown in Fig. 3(d), that is concentrated near the points where $k_x, k_y = \pm\varphi$. The eigenfrequencies of even eigenmodes satisfy the analytical Fabry-Pérot-like equation [15,16] $\rho(\varepsilon) e^{iK(\varepsilon)(N+1)} = 1$. Looking for the solution to this equation with $K \approx \varphi + i\,\mathrm{Im}\, K$, we obtain the following approximate analytical equation for the decay rate of the brightest state:

$$-\frac{\mathrm{Im}\,\varepsilon}{\gamma_{1D}} \approx \frac{N}{W(2N\,\sin\varphi)}, \tag{8}$$

where $W(x)$ is the Lambert $W$ function defined by the equation $W\, e^W = x$. For large $N$ we use the approximation for the

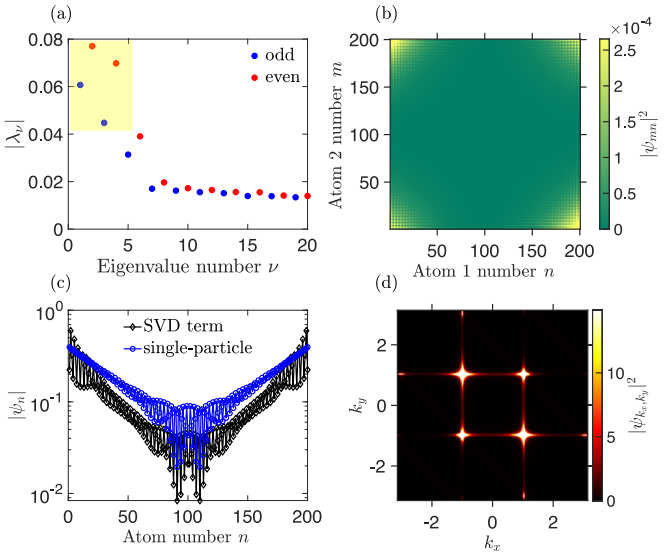


FIG. 3. Origin of distant bound states. (a) Largest singular values $\lambda$ entering the SVD expansion Eq. (6) of the distant bound state No. 2 from Fig. 2. Red and blue dots correspond to even and odd singular vectors, respectively. (b) Approximated wave function of the distant bound state No. 2 calculated including only four largest singular values in Eq. (6), indicated by the yellow rectangle in panel (a). (c) Distribution of the wave function corresponding to the largest odd SVD term and the single-particle wave function of the brightest state. (d) Color map of the two-dimensional Fourier transform of the wave function of the distant bound state No. 2.

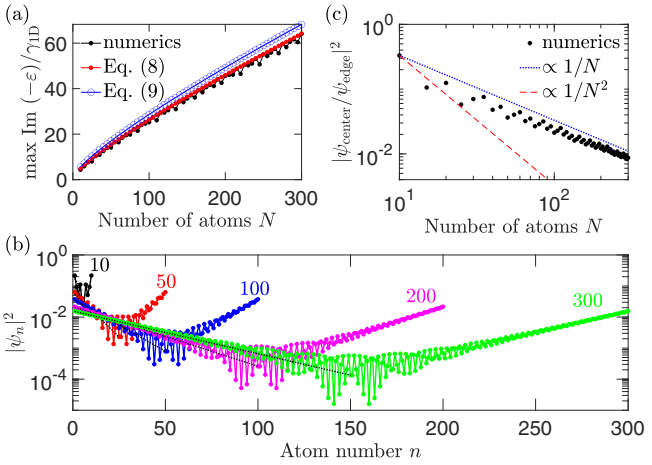


FIG. 4. Scaling of single-particle eigenstates. (a) Dependence of the radiative decay rate of the brightest state on the number of atoms $N$ calculated numerically and analytically following Eqs. (8) and (9). (b) Wave function of the brightest state depending on the length of the array, shown on the graph. Black dotted lines show the exponential decay extrapolated from the edge of the structure to its center. (c) Center-to-edge ratio of the probabilities depending on the number of atoms $N$. Dotted blue and dashed red lines show the asymptotic laws $1/N$ and $1/N^2$. Other calculation parameters are the same as in Fig. 2.

Lambert function, which yields

$$-\frac{\mathrm{Im}\,\varepsilon}{\gamma_{1D}} \approx \frac{N}{\ln(2N\,\sin\varphi) - \ln\ln(2N\,\sin\varphi)}. \tag{9}$$

The dependence of the radiative decay on the array length, calculated numerically and analytically following Eqs. (8) and (9), is shown in Fig. 4(a). The decay rate increases with the number of atoms almost linearly due to the weak logarithmic growth of the Lambert function and the corresponding eigenstate can be considered as a superradiant one. Due to the radiative decay, the superradiant states have a large imaginary part of the polariton wave vector $\mathrm{Im}\,K(\varepsilon) > 0$ and, according to Eq. (7), this leads to the decay of the wave function from the edges towards the structure center, which is caused solely by the radiative losses. The wave function of the brightest state calculated for arrays of different lengths is shown in Fig. 4(b) and indeed falls exponentially from the edges to the center. An important observation from Fig. 4(b) is that the slope of the dependence $\ln|\psi_n|$ on $n$ becomes smaller with the increase of the array length $N$. The probability of finding the polariton in the center is $\sim N$ times smaller than at the edge, $|\psi_{center}/\psi_{edge}|^2 \equiv |\psi_{N/2}/\psi_1|^2 \propto 1/N$. In order to check this numerically we have fitted the exponential decay of the wave function from the edge to the center for each value of $N$ and extrapolated it to the center of the structure. The corresponding fits are shown by black dotted lines in Fig. 4(b). Such extrapolation allows us to determine the value of $|\psi_{N/2}|^2$ in a way that is robust to the oscillations of the wave function. Next, we have plotted in Fig. 4(c) the ratio $|\psi_{center}/\psi_{edge}|^2$ depending on $N$ in a double logarithmic scale that clearly agrees with the $1/N$ decay law, shown by the dotted blue line. This $1/N$ suppression is in stark contrast to the conventional edge state where the ratio $|\psi_{N/2}/\psi_1|^2$ decays exponentially with $N$ as $|\psi_{N/2}/\psi_1|^2 = \exp(-N/l_{loc})$, where the localization length $l_{loc}$ is independent of $N$. In the considered case $l_{loc}$ is not constant but increases with $N$, which is a direct manifestation of the non-Hermitian nature of the problem. For larger $N$ the radiative decay due to the photon escape through the edges becomes relatively less important and the localization is suppressed. The result that $|\psi_{center}/\psi_{edge}|^2 \propto 1/N$ can also be viewed as a signature of a substantial admixture of the scattering states, which are delocalized in space, to the edge states in Fig. 4. It is this admixture that helps the two photons to repel each other and form a bound distant state, with two photons localized on the opposite edges. The discussed scaling of the localization is reflected in the eigenfrequency of the superradiant state found from Eq. (8) that approximately satisfies the equation $e^{-(N-1)\,\mathrm{Im}\,K(\varepsilon)} \approx 1/(N\,\sin\varphi)$, which means linear, rather than exponential, suppression of the probability in the center of the structure.

## III. ROBUSTNESS AGAINST THE DISORDER

In order to investigate the stability of the distant bound states against the short-range disorder we add the following interaction term to the Hamiltonian Eq. (4):

$$V = \gamma_{1D} \sum_{n=1}^{N-1} \chi_n (\sigma_n^\dagger \sigma_n)(\sigma_{n+1}^\dagger \sigma_{n+1}). \tag{10}$$

Physically, such short-range interactions occur, e.g., due to van der Waals couplings between the atoms and they can also be implemented for superconducting qubits [17]. Here,

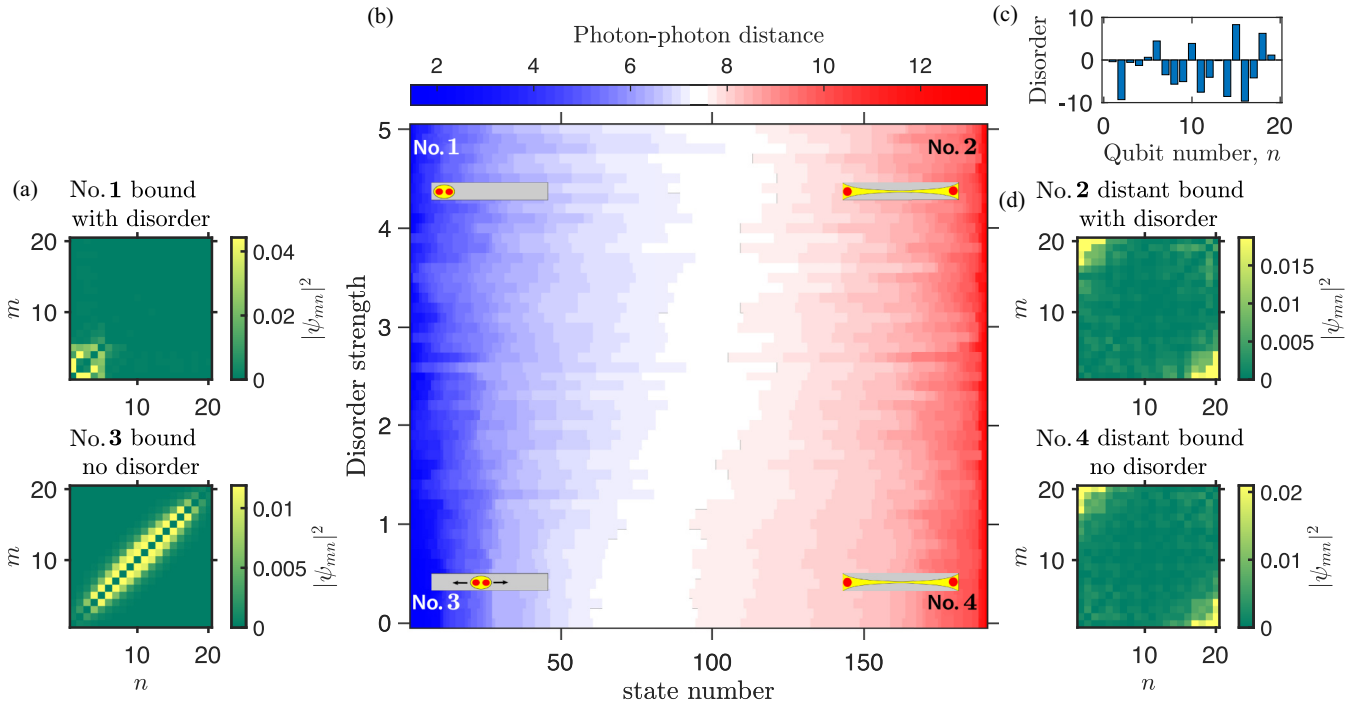


FIG. 5. Effect of disorder. [(a),(d)] Wave functions of four characteristic two-photon states. (b) Dependence of the photon-photon distances on the disorder strength $\chi$. Each horizontal line in the calculated 2D map corresponds to a single disorder realization. All the $N(N-1)/2$ eigenstates have been sorted according to the average photon-photon distance $p$ defined by Eq. (5). (c) Distribution of the disorder amplitudes $\chi_n$ for the largest disorder strength $\chi = 5$. Calculation has been performed for $N = 20$ and $\omega_0 d/c = 1$.

the coefficients $\chi_n$, characterizing the disorder strength, are independent random variables with zero mean value and the dispersion $\langle \chi_n^2 \rangle \equiv \chi^2$; see Fig. 5(c) for a particular realization. The calculated dependence of the average photon-photon distance on the disorder strength is shown in Fig. 5. For vanishing disorder, one can clearly distinguish the bound two-photon states with the small distance $p$ [state No. 3 in Fig. 5(a)] and the distant bound states [state No. 4 in Fig. 5(b)]; see also the histogram Fig. 2(c). For bound states, two photons propagate together and their center-of-mass wave function forms a standing wave in the structure. These bound photon pairs are rather sensitive to the short-range disorder Eq. (10). The increase of the disorder strength leads to the localization of the bound pairs; see the state No. 1 in Fig. 5(a). On the other hand, the distant bound states that we focus on are significantly less sensitive to the short-range interactions due to the increased photon-photon distance. This is evident from the persistence of the red-colored states with the large distance in the right edge of the diagram in Fig. 5(b). The most distant state is weakly affected by the disorder, as can be seen by comparing the wave functions No. 2 and No. 4 in Fig. 5(b). Such robustness against the disorder has a certain similarity to the Majorana fermions in Kitaev's model [18], which were predicted to arise at the edges of a nanowire put upon a superconductor in a magnetic field [19]. A pair of such Majorana states localized on the opposite edges of the wire forms a single ordinary fermionic excitation with zero energy. The latter appears to be partially immune to dephasing because its two Majorana components cannot be mixed by a short-range perturbation, such as, e.g., Coulomb interaction [18,20]. However, even despite certain robustness to the disorder the considered states have very short radiative lifetime, since they originate from atom-photon interactions.

## IV. SUMMARY AND OUTLOOK

In this section, we try to present a bird's-eye view of the two-photon quantum states in the finite array of atoms coupled to a waveguide. Schematic spatial false-color maps of two-photon joint probabilities $|\Psi(x_1, x_2)|^2$ are presented in the schematic diagram in Fig. 6. They are grouped depending on the relative distance between the two photons (a larger distance corresponds to the upper panels) and depending on whether the photons are located mostly at the structure edges (right panels) or in the bulk (left panels). The bulk states are most simple to understand. They are limited to the scattering states, where two photons are delocalized in space and are quasi-independent from each other [Fig. 6(b)], fermionized states with increased radiative lifetime [Fig. 6(a)] [21], where the average photon-photon distance is increased, and bound photon pairs [Fig. 6(c)] [22–24]. To the best of our knowledge, neither fermionized states nor bound states have been directly observed in experiments yet. However, the bound states are well known in other setups. They have been observed for cold atoms in optical lattices [25], correlated two-photon quantum walks have recently been experimentally studied for superconducting quantum processors [26], and even three- photon bound states were seen for light interacting with Rydberg atomic states [27,28]. Moreover, tunable photon bunching and antibunching, recently realized in the WQED setup with cold atoms coupled to the nanofiber [29], is in fact mediated by the two-photon bound states [30–36]. Thus direct experimental

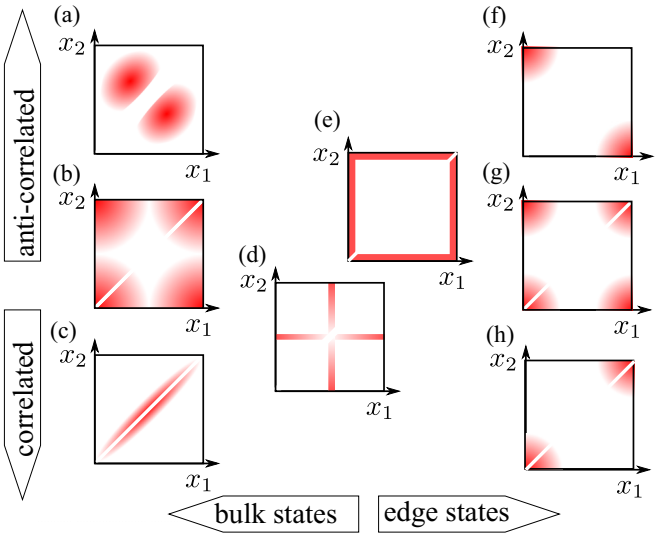


FIG. 6. Types of two-photon states. The diagrams schematically illustrate two-photon wave function $|\Psi(x_1, x_2)|^2$ in a finite array of atoms depending on the first and second photon coordinates. The states are grouped depending on whether the two photons are correlated or anticorrelated in space and located in the bulk of the structure or at its edges. The distant bound state, considered in this work, corresponds to panel (f).

observation of the two-photon bound states does not seem to be in the realm of impossible for state-of-the-art setups. The most advantageous platform should probably be based on superconducting qubits, since it allows access (excitation and probing) of individual qubits [37]. As demonstrated by the calculation in Fig. 5, the array of 20 qubits should already be sufficient to observe the bound states as well as other quantum states discussed below. Figures 6(d) and 6(e) present unusual types of two-photon quantum states, predicted in our previous works [38–40]. They manifest interaction-induced localization when one of the two indistinguishable photons forms a standing wave that induces a trapping potential for the other photon. This second photon can be localized either in the center [Fig. 6(d)] or at the edge [Fig. 6(e)] of the array. Since the standing wave is delocalized, such states can be considered as lying in between bulk and edge states; for example, for the state in Fig. 6(e), one of the photons is always in the bulk while another one is always at the edge. The two photons can be both correlated and anticorrelated in space depending on whether the trapping is in the antinode or in the node of the standing wave. Thus, while being quite interesting from the fundamental side, the states in Figs. 6(d) and 6(e) do not seem optimal to enhance or suppress the photon-photon spatial correlations. Finally, we proceed to the states in Figs. 6(f), 6(g), and 6(h), where both photons are at the edges of the array. Depending on the specifics of two-photon interactions, the photon pair can be quasi-independent [Fig. 6(g)], correlated [Fig. 6(h)], or anticorrelated [Fig. 6(f)]. As discussed above, the latter state, put forward in this work, is the most robust against short-range interactions between the photons.

To summarize, waveguide quantum electrodynamics, which has become a separate research field only relatively recently, is a very promising platform to control two-photon correlations [29]. Even the simplest two-body problem in WQED manifests a number of quite unusual two-photon states. It is not clear whether our classification in Fig. 6 is complete and how it can be extended for a larger number of particles [41] or even in the many-body regime [42], but we can expect beautiful fundamental phenomena that will also be hopefully soon complemented by experimental demonstrations and even practical applications for the emerging quantum industry. It also remains an important standing question how to probe complicated correlated states in an experiment, especially if their radiative lifetime is very long, as in the case of subradiant states, or if it is very short, as in the considered case. One of the potential directions to apply considered states could be the quantum state transfer. For example, Ref. [43] has recently experimentally demonstrated quantum state transfer between edge-localized topological states in a structured waveguide. If the qubits storing quantum information are coupled to the considered edge-localized states, the edge-localized states could then mediate the transfer.

## ACKNOWLEDGMENTS

The work of A.V.P. was supported by Rosatom in the framework of the Roadmap for Quantum computing (Contracts No. 868-1.3-15/15-2021 and No. R2152). A.V.P. also acknowledges partial support from the Foundation “Basis”.

[1] E. H. Lieb and W. Liniger, Exact analysis of an interacting Bose gas. I. The general solution and the ground state, Phys. Rev. **130**, 1605 (1963).

[2] E. L. Ivchenko and G. E. Pikus, *Superlattices and Other Heterostructures: Symmetry and Optical Phenomena* (Springer-Verlag, Berlin, 1997).

[3] R. A. Pinto, M. Haque, and S. Flach, Edge-localized states in quantum one-dimensional lattices, Phys. Rev. A **79**, 052118 (2009).

[4] M. A. Gorlach and A. N. Poddubny, Topological edge states of bound photon pairs, Phys. Rev. A **95**, 053866 (2017).

[5] V. Pouthier, Boundary-induced energy localization in a nonlinear quantum lattice, Phys. Rev. B **76**, 224302 (2007).

[6] M. Haque, Self-similar spectral structures and edge-locking hierarchy in open-boundary spin chains, Phys. Rev. A **82**, 012108 (2010).

[7] E. R. Christensen, A. Camacho-Guardian, O. Cotlet, A. Imamoglu, M. Wouters, G. M. Bruun, and I. Carusotto, Microscopic theory of cavity-enhanced interactions of dipolaritons, arXiv:2212.02597.

[8] D. Roy, C. M. Wilson, and O. Firstenberg, *Colloquium:* strongly interacting photons in one-dimensional continuum, Rev. Mod. Phys. **89**, 021001 (2017).

[9] D. E. Chang, J. S. Douglas, A. González-Tudela, C.-L. Hung, and H. J. Kimble, *Colloquium:* Quantum matter built from

nanoscopic lattices of atoms and photons, Rev. Mod. Phys. **90**, 031002 (2018).

[10] A. S. Sheremet, M. I. Petrov, I. V. Iorsh, A. V. Poshakinskiy, and A. N. Poddubny, Waveguide quantum electrodynamics: Collective radiance and photon-photon correlations, Rev. Mod. Phys. **95**, 015002 (2023).

[11] N. V. Corzo, J. Raskop, A. Chandra, A. S. Sheremet, B. Gouraud, and J. Laurat, Waveguide-coupled single collective excitation of atomic arrays, Nature (London) **566**, 359 (2019).

[12] B. Kannan, A. Almanakly, Y. Sung, A. Di. Paolo, D. A. Rower, J. Braumüller, A. Melville, B. M. Niedzielski, A. Karamlou, K. Serniak, A. Vepsäläinen, M. E. Schwartz, J. L. Yoder, R. Winik, J. I.-J. Wang, T. P. Orlando, S. Gustavsson, J. A. Grover, and W. D. Oliver, On-demand directional microwave photon emission using waveguide quantum electrodynamics, Nat. Phys. **19**, 394 (2023).

[13] T. Caneva, M. T. Manzoni, T. Shi, J. S. Douglas, J. I. Cirac, and D. E. Chang, Quantum dynamics of propagating photons with strong interactions: A generalized input–output formalism, New J. Phys. **17**, 113001 (2015).

[14] M. Voronov, E. Ivchenko, M. Erementchouk, L. Deych, and A. Lisyansky, Photoluminescence spectroscopy of one-dimensional resonant photonic crystals, J. Lumin. **125**, 112 (2007).

[15] G. Fedorovich, D. Kornovan, A. Poddubny, and M. Petrov, Chirality-driven delocalization in disordered waveguide-coupled quantum arrays, Phys. Rev. A **106**, 043723 (2022).

[16] A. V. Poshakinskiy and A. N. Poddubny, Quantum Borrmann effect for dissipation-immune photon-photon correlations, Phys. Rev. A **103**, 043718 (2021).

[17] P.-O. Guimond, B. Vermersch, M. L. Juan, A. Sharafiev, G. Kirchmair, and P. Zoller, A unidirectional on-chip photonic interface for superconducting circuits, npj Quantum Inf. **6**, 32 (2020).

[18] A. Yu. Kitaev, Unpaired Majorana fermions in quantum wires, Phys. Usp. **44**, 131 (2001).

[19] Y. Oreg, G. Refael, and F. von Oppen, Helical Liquids and Majorana Bound States in Quantum Wires, Phys. Rev. Lett. **105**, 177002 (2010).

[20] F. Wilczek, Majorana returns, Nat. Phys. **5**, 614 (2009).

[21] Yu.-X. Zhang and K. Mølmer, Theory of Subradiant States of a One-Dimensional Two-Level Atom Chain, Phys. Rev. Lett. **122**, 203605 (2019).

[22] Yu.-X. Zhang, C. Yu, and K. Mølmer, Subradiant bound dimer excited states of emitter chains coupled to a one dimensional waveguide, Phys. Rev. Res. **2**, 013173 (2020).

[23] A. N. Poddubny, Quasiflat band enabling subradiant two-photon bound states, Phys. Rev. A **101**, 043845 (2020).

[24] G. Calajó and D. E. Chang, Emergence of solitons from many-body photon bound states in quantum nonlinear media, Phys. Rev. Res. **4**, 023026 (2022).

[25] K. Winkler, G. Thalhammer, F. Lang, R. Grimm, J. Hecker Denschlag, A. J. Daley, A. Kantian, H. P. Büchler, and P. Zoller, Repulsively bound atom pairs in an optical lattice, Nature (London) **441**, 853 (2006).

[26] Z. Yan, Yu.-R. Zhang, M. Gong, Y. Wu, Y. Zheng, S. Li, C. Wang, F. Liang, J. Lin, Yu. Xu, C. Guo, L. Sun, C.-Z. Peng, K. Xia, H. Deng, H. Rong, J. Q. You, F. Nori, H. Fan, X. Zhu *et al.*, Strongly correlated quantum walks with a 12-qubit superconducting processor, Science **364**, 753 (2019).

[27] Qi.-Yu. Liang, A. V. Venkatramani, S. H. Cantu, T. L. Nicholson, M. J. Gullans, A. V. Gorshkov, J. D. Thompson, C. Chin, M. D. Lukin, and V. Vuletić, Observation of three-photon bound states in a quantum nonlinear medium, Science **359**, 783 (2018).

[28] L. Drori, B. C. Das, T. D. Zohar, G. Winer, E. Poem, A. Poddubny, and O. Firstenberg, Quantum vortices of strongly interacting photons, Science **381**, 193 (2023).

[29] A. S. Prasad, J. Hinney, S. Mahmoodian, K. Hammerer, S. Rind, P. Schneeweiss, A. S. Sørensen, J. Volz, and A. Rauschenbeutel, Correlating photons using the collective nonlinear response of atoms weakly coupled to an optical mode, Nat. Photon. **14**, 719 (2020).

[30] J.-T. Shen and S. Fan, Strongly Correlated Two-Photon Transport in a One-Dimensional Waveguide Coupled to a Two-Level System, Phys. Rev. Lett. **98**, 153003 (2007).

[31] V. I. Yudson and P. Reineker, Multiphoton scattering in a one-dimensional waveguide with resonant atoms, Phys. Rev. A **78**, 052713 (2008).

[32] T. Shi and C. P. Sun, Lehmann-Symanzik-Zimmermann reduction approach to multiphoton scattering in coupled-resonator arrays, Phys. Rev. B **79**, 205111 (2009).

[33] D. Roy, Few-photon optical diode, Phys. Rev. B **81**, 155117 (2010).

[34] H. Zheng, D. J. Gauthier, and H. U. Baranger, Waveguide QED: Many-body bound-state effects in coherent and Fock-state scattering from a two-level system, Phys. Rev. A **82**, 063816 (2010).

[35] A. Albrecht, L. Henriet, A. Asenjo-Garcia, P. B. Dieterle, O. Painter, and D. E. Chang, Subradiant states of quantum bits coupled to a one-dimensional waveguide, New J. Phys. **21**, 025003 (2019).

[36] S. Mahmoodian, G. Calajó, D. E. Chang, K. Hammerer, and A. S. Sørensen, Dynamics of Many-Body Photon Bound States in Chiral Waveguide QED, Phys. Rev. X **10**, 031011 (2020).

[37] M. Zanner, T. Orell, C. M. F. Schneider, R. Albert, S. Oleschko, M. L. Juan, M. Silveri, and G. Kirchmair, Coherent control of a multi-qubit dark state in waveguide quantum electrodynamics, Nat. Phys. **18**, 538 (2022).

[38] J. Zhong, N. A. Olekhno, Y. Ke, A. V. Poshakinskiy, C. Lee, Y. S. Kivshar, and A. N. Poddubny, Photon-Mediated Localization in Two-Level Qubit Arrays, Phys. Rev. Lett. **124**, 093604 (2020).

[39] A. V. Poshakinskiy, J. Zhong, Y. Ke, N. A. Olekhno, C. Lee, Y. S. Kivshar, and A. N. Poddubny, Quantum Hall phases emerging from atom–photon interactions, npj Quantum Inf. **7**, 34 (2021).

[40] A. V. Poshakinskiy, J. Zhong, and A. N. Poddubny, Quantum Chaos Driven by Long-Range Waveguide-Mediated Interactions, Phys. Rev. Lett. **126**, 203602 (2021).

[41] J. Zhong and A. N. Poddubny, Classification of three-photon states in waveguide quantum electrodynamics, Phys. Rev. A **103**, 023720 (2021).

[42] N. Fayard, L. Henriet, A. Asenjo-Garcia, and D. E. Chang, Many-body localization in waveguide quantum electrodynamics, Phys. Rev. Res. **3**, 033233 (2021).

[43] E. Kim, X. Zhang, V. S. Ferreira, J. Banker, J. K. Iverson, A. Sipahigil, M. Bello, A. González-Tudela, M. Mirhosseini, and O. Painter, Quantum Electrodynamics in a Topological Waveguide, Phys. Rev. X **11**, 011015 (2021).